

Research Article

An Exponential Varying-Parameter Neural Network for Repetitive Tracking of Mobile Manipulators

Ying Kong , Qingqing Tang, Jingsheng Lei , and Ruiyang Zhang

Department of Information and Electronic Engineering, Zhejiang University of Science and Technology, Hangzhou, China

Correspondence should be addressed to Jingsheng Lei; jshlei@126.com

Received 11 June 2020; Revised 17 July 2020; Accepted 20 July 2020; Published 15 September 2020

Guest Editor: Qiang Chen

Copyright © 2020 Ying Kong et al. This is an open access article distributed under the Creative Commons Attribution License, which permits unrestricted use, distribution, and reproduction in any medium, provided the original work is properly cited.

A novel exponential varying-parameter neural network (EVPNN) is presented and investigated to solve the inverse redundancy scheme of the mobile manipulators via quadratic programming (QP). To suspend the phenomenon of drifting free joints and guarantee high convergent precision of the end effector, the EVPNN model is applied to trajectory planning of mobile manipulators. Firstly, the repetitive motion scheme for mobile manipulators is formulated into a QP index. Secondly, the QP index is transformed into a time-varying matrix equation. Finally, the proposed EVPNN method is used to solve the QP index via the matrix equation. Theoretical analysis and simulations illustrate that the EVPNN solver has an exponential convergent speed and strong robustness in mobile manipulator applications. Comparative simulation results demonstrate that the EVPNN possesses a superior convergent rate and accuracy than the traditional ZNN solver in repetitive trajectory planning with a mobile manipulator.

1. Introduction

Robotic arms have attracted increasing attention in engineering applications. Various algorithms and methodologies have been investigated for the kinematics of the robotic arms. Among the existed robot arms, redundant manipulators have played an enormous role in industrial control for repeatable dull work, such as equipping [1], automation [2, 3], and manufacturing [4, 5]. A manipulator is defined as redundancy when the degrees of freedom (DOF) are more than the minimum required to fulfil a given task by the end effector. One of the most important issues in the operating space is the redundancy resolution that is the solutions for trajectory of each free joint vector when a primary task of the end effector is given in the Cartesian path. The redundant DOF produces infinite feasible solutions to redundancy resolution schemes. For example, multiobjective grabbing is studied in motion planning of redundant manipulators, which utilized the closed-loop pseudo-inverse technology and a genetic inherit algorithm [6–8]. Minimum velocity optimization based on pseudo-inverse focusing on decreasing the sum of squares of joint velocities is investigated

in [8]. However, it cannot guarantee the non-singularities of each joint angle. Moreover, the repetitiveness of the end effector with the redundant manipulator may not be realized.

To obtain widely flexible operation space for special tasks, algorithms about kinematics of the mobile manipulators have been studied by industry, military, and aerospace control [9, 10]. The integration of a mobile manipulator consists of a mobile platform and a robot manipulator upside. How to coordinate the given task with the gross movement completed by the mobile base is a comprehensive problem. It is a challenge subject to realize repetitiveness of a mobile manipulator on the inverse motion scheme. Tchon firstly exploited an endogenous configuration algorithm for repetitive kinematics of the mobile manipulators [11]. Further investigations about the spatial vector and extended Jacobian for inverse kinematics of the mobile manipulator are presented in [12–14]. With the development of neural networks, various solutions have been shown due to the distributed storage, adaptive capability, and easy implementation. He et al. proposed an adaptive neural network model for rehabilitation with unknown kinematic system

[15]. In [16], a unknown model with Jacobian matrix adaption for repetitive control was presented. For unknown dynamic systems, various optimization programming of parameter estimation via the neural network model are studied with the condition of friction compensation and fuzzy control [17–19]. In [20], a feasible controller for a flexible mobile manipulator system concerning the kinematic vibration was designed. A great deal of recurrent neural network (RNN) is mainly focusing online solution for time-varying problems. Among these neural solutions, a systematic methodology of the Zhang neural network (ZNN) gradually formalized since 2008 [21–23]. Despite of the success contribution of ZNN models, the convergent time of the dynamic ZNN is infinite, which is not satisfying the situation for real-time processing. A serial of finite time neural network models are presented to accelerate the convergent speed [24–28]. Considering the joint limitation of the mobile manipulator, an energy minimization resolution via the velocity variable and accelerated velocity variable was established to guarantee the norm of the velocity to zero and realize repetitiveness of mobile manipulators [29]. Overall, the scaling parameter in the existed neural models is fixed, which needs to be adjusted as large to eliminate the convergent time. Most of the dynamics are focusing on the activation function of the neural network; few research studies are considering the varying coefficient of the neural networks.

Kinematic control of the robot arm via neural networks is a popular trend for different trajectory tracking. To remedy the drifting joint phenomenon, an extended motion scheme at the joint-velocity level has been proposed [30]. In [31], a neural dynamic method is exploited for repetitive kinematics of a dual-arm manipulator. With the development of neural dynamics, neural network technologies in cooperative control of multiple manipulators have been sprung up. A distributed task allocation from the perspective of competitive control for multiple manipulators was proposed in [32]. Recurrent neural networks for distributed multiple manipulators have been evaluated in executing the given tasks [33].

However, the position rehabilitation of each joint of the robotic arms is an important direction in robotic kinematics, which can avoid joint-physical limitation and realize repeatable motion task. This is our main motivation for the present research. To satisfy the faster convergent requirement, different from the fixed parameter neural network model such as ZNN, an exponential varying-parameter neural network (EVPNN) is constructed in this paper. It is noted as varying-parameter neural network because the scaling parameter of the EVPNN is varying with time. It is necessary to point out that the proposed EVPNN is prompt to solve complex online optimization, such as trajectory planning of a mobile manipulator.

The remainder of this paper is organized as follows. Section 2 gives the kinematic formulation of the mobile manipulator. In Section 3, an EVPNN model is constructed and analyzed for solving the repetitive kinematic scheme. Simulation results on a mobile manipulator with three wheels are shown in Section 4. Section 5 concludes the paper.

The main contributions of this manuscript are highlighted as follows:

- (1) A novel EVPNN is presented and analyzed to solve the repetitive trajectory tracking of mobile manipulators under external noises. It is the first time to construct such an EVPNN model for solving this inverse redundancy scheme.
- (2) Theoretical analysis proves that the novel EVPNN can reduce to zero in exponential convergent rate and obtain high convergent precision.
- (3) Simulation comparisons between the EVPNN and the ZNN illustrate the exponential convergent rate, higher convergent accuracy, and strong robustness of the EVPNN when both neural solutions are applied to realize the repeatable motion of mobile manipulators.

2. Fundamentals, Scheme, and QP Formulation

Kinematic analysis of the manipulator is demonstrated in experiments with the seven-DOF (degree-of-freedom) mobile-base PA10 robot. PA10 robotic arm in [34] is composed of three links, connected together by a set of joints. Moreover, the mechanical arm can move flexibly by adding three Swedish wheels to the base, thus breaking the space limitation.

2.1. Redundant Manipulator Kinematics. For mobile manipulators, the issue of kinematics can be described as studying the relation between the movement of each joint angle and the pose of the end effector without considering torques for the motor system. The forward kinematic equation is as follows:

$$r(t) = f(\theta(t)), \quad (1)$$

where $\theta(t) \in R^n$ denotes the joint angle vector of an n -DOF manipulator with respect to time t . $r(t) \in R^m$ denotes the end-effector's position vector in the m -dimensional Cartesian space. Besides, it also reaches consensus on $n > m$. When given a specific construct of the robot arm and some parameters about it, forward-kinematics mapping function $f(\cdot): R^n \rightarrow R^m$ can be obtained.

According to the definition of equation (1), the inverse kinematic equation at the velocity level is considered as follows:

$$\dot{r}(t) = J(\theta(t))\dot{\theta}(t), \quad (2)$$

where $J(\theta(t)) = \partial f(\theta(t))/\partial \theta(t)$, and $J(\theta(t)) \in R^{m \times n}$ is called the Jacobian matrix. $\dot{r}(t) = dr(t)/dt$ and $\dot{\theta}(t) = d\theta(t)/dt$ denote the velocity and joint velocity, respectively.

2.2. Kinematic Analysis of the Mobile Platform. We now consider a mobile platform with three Swedish wheels, and the geometric analysis of the mobile base in the global

coordinate system is depicted in Figure 1. In [35], the motion constraint is described as

$$\begin{bmatrix} \dot{P}_A \\ \dot{\alpha} \end{bmatrix} = \begin{bmatrix} M_2 \\ M_1 \end{bmatrix} \times \dot{\rho}, \quad (3)$$

where $P_A = [x_A, y_A]^T$ is the coordinate of center point A of the mobile platform on the x -axis and y -axis. Consider that wheels in this paper do not move in the z -axis direction, so $z_A = 0$. Furthermore, \dot{P}_A is the time derivative of P_A . α denotes the heading angle of the removable base, and $\dot{\alpha}$ is the angular velocity. In addition,

$$M_2 = \frac{2r}{3} \begin{bmatrix} -\sin \alpha & -\sin\left(\frac{\pi}{3} - \alpha\right) & \sin\left(\frac{\pi}{3} + \alpha\right) \\ \cos \alpha & -\cos\left(\frac{\pi}{3} - \alpha\right) & -\cos\left(\frac{\pi}{3} + \alpha\right) \end{bmatrix}, \quad (4)$$

$$M_1 = \begin{bmatrix} r & r & r \\ 3l & 3l & 3l \end{bmatrix}, \quad (5)$$

$$\dot{\rho} = [\dot{\rho}_1, \dot{\rho}_2, \dot{\rho}_3]^T, \quad (6)$$

where r denotes the radius of three wheels with the same structure and l denotes the distance between center point A and wheel. Then, $\dot{\rho}_1$, $\dot{\rho}_2$, and $\dot{\rho}_3$ represent rotation speeds of three wheels, respectively.

2.3. Integration Analysis of the Wheeled Mobile Robot. As for the PA10 robot ($m = 3$ and $n = 7$) with the wheeled platform, the position of the end actuator is constrained by the heading angle and seven joint angles as follows:

$$r_G = \begin{bmatrix} x_G \\ y_G \\ z_G \end{bmatrix} = R(\alpha)f(\theta(t)) + \begin{bmatrix} P_A \\ 0 \end{bmatrix}, \quad (7)$$

where r_G denotes the position of the end effector based on the global coordinate system $\{O_G - X_G Y_G Z_G\}$. $R(\alpha)$ is an orthogonal rotation matrix between the mobile base and the robot arm, which is formulated as

$$R(\alpha) = \begin{bmatrix} \cos \alpha & -\sin \alpha & 0 \\ \sin \alpha & \cos \alpha & 0 \\ 0 & 0 & 1 \end{bmatrix}. \quad (8)$$

Evaluate the derivative of equation (7) with respect to time after letting $F(\alpha, \theta) = R(\alpha)f(\theta(t))$, that is,

$$\dot{r}_G = \frac{\partial F(\alpha, \theta)}{\partial \beta} \cdot \frac{d\beta}{dt} + \begin{bmatrix} \dot{P}_A \\ 0 \end{bmatrix}, \quad (9)$$

where $\beta = [\alpha, \theta]^T$. Then,

$$\dot{r}_G = J(\alpha, \theta) \begin{bmatrix} \dot{\alpha} \\ \dot{\theta} \end{bmatrix} + \begin{bmatrix} \dot{P}_A \\ 0 \end{bmatrix}, \quad (10)$$

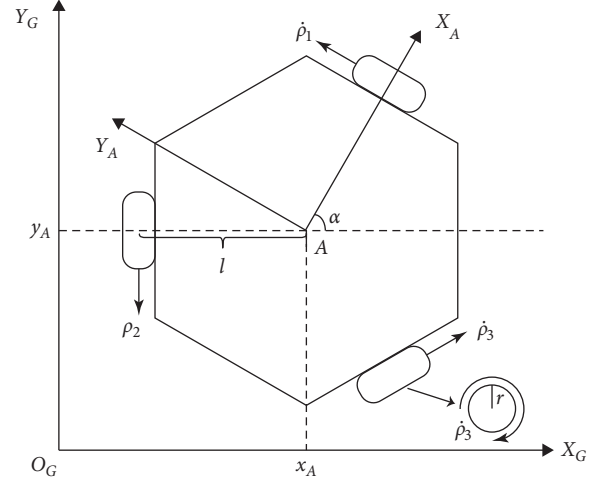


FIGURE 1: The structure of the mobile platform in the global coordinate system.

where $J(\alpha, \theta) = \partial F(\alpha, \theta)/\partial \beta \in R^{3 \times 8}$. As mentioned before in Section 2.2, $\dot{P}_A = M_2 \dot{\rho}$ and $\dot{\alpha} = M_1 \dot{\rho}$. We have

$$\dot{r}_G = \left(J(\alpha, \theta) \begin{bmatrix} M_1 & 0 \\ 0 & I \end{bmatrix} + \begin{bmatrix} M_2 & 0 \\ 0 & 0 \end{bmatrix} \right) \begin{bmatrix} \dot{\rho} \\ \dot{\theta} \end{bmatrix}. \quad (11)$$

This is simplified as

$$\dot{r}_G = M \dot{\Theta}, \quad (12)$$

where $\Theta = [\rho; \theta] \in R^{10 \times 1}$.

With regard to a redundant mobile PA10 robot, when performing a series of complex tasks repeatedly, the path crossed by the manipulator must be closed, which means each joint angle of the end effector must eventually return to the original position. On the contrary, we aim to research a method to minimize the joint displacement between the current and initial status under the above condition. Therefore, consider the following repetitive motion optimal scheme:

$$\text{minimize } \frac{1}{2} \|Q \dot{\Theta} + \sigma\|_2^2 \quad (13)$$

$$\text{subject to } M \dot{\Theta} = \dot{r}_G^* + k(r_G^* - r_G),$$

where $Q = [Q_1 \ 0; 0 \ I] \in R^{10 \times 10}$ with I being a seven-dimensional identity matrix, and $Q_1 = [M_1 \cos \alpha; M_2]$. Moreover, $\sigma = [\eta_1 \sin((\alpha(t))) - \sin((\alpha(0))); \eta_2 (P_A(t) - P_A(0)); \eta_3 (\theta(t) - \theta(0))] \in R^{10 \times 1}$, in which three configurable parameters $\eta_1, \eta_2, \eta_3 > 0$ and so is k in equation (13). r_G^* denotes the ideal path of the manipulator. Furthermore, the criterion of the repetitive motion scheme can be expanded as

$$\frac{1}{2} \|Q \dot{\Theta} + \sigma\|_2^2 = \frac{1}{2} \dot{\Theta}^T Q^T Q \dot{\Theta} + \sigma^T Q \dot{\Theta} + \frac{1}{2} \sigma^T \sigma. \quad (14)$$

Note that $\dot{\Theta}^T Q^T \sigma = \sigma^T Q \dot{\Theta}$. Given that $\sigma^T \sigma$ does not play a critical role in equation (13), this paper decides to omit it, reducing the complexity of the calculation process. Besides,

we set the analytic solution $\dot{\Theta}$ as X , $V = Q^T Q$, and $S = Q^T \sigma$. Therefore, equation (13) has been reformulated as

$$\text{minimize } \frac{1}{2} X^T V X + S^T X \quad (15)$$

$$\text{subject to } MX = \dot{r}_G^* + k(r_G^* - r_G).$$

Using the relative Lagrange theorem can solve the above QP (quadratic programming) problem. Firstly, we set $L(X(t), \lambda(t), t) = X^T V X / 2 + S^T X + \lambda^T(t) (MX - \dot{r}_G^* - k(r_G^* - r_G))$ with $\lambda(t) \in R^{3 \times 1}$ denoting the Lagrange-multiplier vector. Then, partial derivation of $L(X(t), \lambda(t), t)$ is evaluated with respect to $X(t)$ and $\lambda(t)$, respectively:

$$\begin{cases} \frac{\partial L(X(t), \lambda(t), t)}{\partial X(t)} = VX + S + M^T \lambda = 0, \\ \frac{\partial L(X(t), \lambda(t), t)}{\partial \lambda(t)} = MX - \dot{r}_G^* - k(r_G^* - r_G) = 0. \end{cases} \quad (16)$$

That is,

$$H(t)Y(t) = G(t), \quad (17)$$

where

$$\begin{aligned} H(t) &= \begin{bmatrix} V(t) & M^T(t) \\ M(t) & O_{3 \times 3} \end{bmatrix} \in R^{13 \times 13}, \\ Y(t) &= \begin{bmatrix} X(t) & \lambda(t) \end{bmatrix} \in R^{13 \times 1}, \\ G(t) &= \begin{bmatrix} -S(t) \\ \dot{r}_G^*(t) + k(r_G^*(t) - r_G(t)) \end{bmatrix} \in R^{13 \times 1}. \end{aligned} \quad (18)$$

3. Time-Varying QP Solver

To approximate the solution of (17), we choose a vector-form error function $E(t) = H(t)Y(t) - G(t)$ to track the time-varying solution $Y(t)$ of equation (17). In other words, $E(t)$ is used to measure the difference between $Y(t)$ and its theoretical solution $Y^*(t)$. The differential equation for $E(t)$ gives

$$\dot{E}(t) = \frac{dE}{dt} = \dot{H}(t)Y(t) + H(t)\dot{Y}(t) - \dot{G}(t). \quad (19)$$

Y. N. Zhang in [22] once came up with the following design formula to monitor time-varying $E(t)$, which is called the ZNN:

$$\dot{E}(t) = -\gamma \Phi(E(t)). \quad (20)$$

With the improvement of (20), an exponential varying-parameter form of such an error vector $E(t)$ is introduced as (termed EVPNN)

$$\dot{E}(t) = -\gamma \psi^{t+a} \Phi(E(t)). \quad (21)$$

There are three regulable constants γ , ψ , and a , which satisfy $\gamma > 0$, $\psi \geq 1$, and $a \geq 0$. Routinely, $\Phi(\cdot)$ denotes the general form of the differentiable activation function, which

is monotonically increasing and odd. Three frequently used $\phi(\cdot)$ (the scalar form of $\Phi(\cdot)$) are selected:

- (1) Linear type, $\phi(e_i) = e_i$, with e_i denoting the i th entry of $E(t)$.
- (2) Biexponential type, $\phi(e_i) = \exp(b e_i) - \exp(-b e_i)$, with $b > 2$.
- (3) Bipolar sigmoid type:

$$\phi(e_i) = \frac{1 + \exp(-\varepsilon)}{1 - \exp(-\varepsilon)} \cdot \frac{1 - \exp(-\varepsilon e_i)}{1 + \exp(-\varepsilon e_i)}, \quad (22)$$

with $\varepsilon \geq 2$ for $0 \leq |e_i| \leq 1$.

At last, applying (21) to repetitive motion planning for the mobile PA10 manipulator, we obtain the following EVPNN model:

$$\begin{aligned} \dot{Y}(t) &= -\dot{H}(t)Y(t) + (I - H(t))\dot{Y}(t) - \gamma \psi^{t+a} \Phi(H(t)Y(t) \\ &\quad - G(t)) + \dot{G}(t). \end{aligned} \quad (23)$$

Figure 2 reveals the implementation process of the EVPNN model (23) thoroughly when solving the repeated motion planning of the mobile manipulator. In this control system, the controller represents the EVPNN model this paper proposed, and plant denotes the problem to be solved.

3.1. Global Stability Analysis

Theorem 1. *Given $H(t)$ and $G(t)$, the solution of $Y(t)$ obtained by model (23) globally converges to the theoretical solution $Y^*(t)$ when applied to solve the repetitive motion problem of the mobile manipulator (13).*

Proof. Firstly, a nonnegative Lyapunov function $v(t)$ is introduced in this part to prove the global stability of model (23), which is designed as

$$v(t) = \frac{\|E(t)\|_2^2}{2} = \frac{E^T(t)E(t)}{2} \geq 0, \quad (24)$$

where $v(t) = 0$ as long as $E(t) = 0$. Then, a derivative of $v(t)$ is taken with respect to time, that is,

$$\dot{v}(t) = E^T(t)\dot{E}(t) = -\gamma \psi^{t+a} \sum_{i=1}^{13} e_i(t)\phi(e_i(t)). \quad (25)$$

Considering $\phi(\cdot)$ is a monotonically increasing odd function, it must satisfy $e_i(t)\phi(e_i(t)) \geq 0$ in equation (25). We have $\dot{v}(t) \leq 0$. By means of Lyapunov's stability theory, the global stability of model (23) for solving repetitive movement is studied. \square

Theorem 2. *Given time-varying matrices $H(t)$ and $G(t)$, the solution of $Y(t)$ obtained by model (23) takes an exponentially convergent rate for the theoretical solution $Y^*(t)$ when applied to solve the repetitive motion problem of the mobile manipulator (13).*

On account of the uncertainty of $B_i(t)$, we cannot judge the positive and negative of $\dot{v}(t)$ directly. Thus, we will analyze the following two situations:

- (1) If $B_i(t) \geq 0$, it follows that $\dot{v}(t) \leq 0$. By means of the Lyapunov stability theorem, it is proved that the error between the analytical solution calculated by disturbed model (33) and the ideal solution converges to zero globally.
- (2) If $B_i(t) < 0$, it will happen that $\dot{v}(t) \leq 0$ or $\dot{v}(t) > 0$. Next, we will focus on the second and worst situation. Supposing that $\phi(|e_i(t)|) = c|e_i(t)|$, where $c \geq 1$, we have

$$\dot{v}(t) \leq -c\gamma\psi^{t+a} \sum_{i=1}^{13} |e_i(t)| \left(|e_i(t)| - \frac{\varphi}{c\gamma\psi^{t+a}} \right) = \sum_{i=1}^{13} Z_i(t), \quad (38)$$

where $Z_i(t) = -c\gamma\psi^{t+a}|e_i(t)|(|e_i(t)| - \varphi/c\gamma\psi^{t+a})$. By deriving $Z_i(t)$ about $|e_i(t)|$, we easily find that $Z_i(t)$ achieves maximum $\varphi^2/4c\gamma\psi^{t+a}$ when $|e_i(t)| = \varphi/2c\gamma\psi^{t+a}$. In addition, $\sum_{i=1}^{13} Z_i(t)$ can also be regarded as the sum of two sets, one is the sum of the top 12 elements $\sum_{i=1}^{12} Z_i(t)$ and the other is the 13th element $Z_{13}(t)$. Now, assume that

$$Z_i(t) = \frac{\varphi^2}{4c\gamma\psi^{t+a}}, \quad \forall i = 1, 2, \dots, 12. \quad (39)$$

There is no doubt that $\sum_{i=1}^{12} Z_i(t)$ is maximal in this case. It will follow that

$$\sum_{i=1}^{13} Z_i(t) = -c\gamma\psi^{t+a}|e_{13}(t)|^2 + \varphi|e_{13}(t)| + \frac{3\varphi^2}{c\gamma\psi^{t+a}}. \quad (40)$$

Since the previous assumption is that the upper bound of $\dot{v}(t)$ is positive, that is to say, $\sum_{i=1}^{13} Z_i(t) > 0$. Consequently, for each $i \in [1, 13]$, we have

$$\max|e_i(t)| \leq \frac{(1 + \sqrt{13})\varphi}{2c\gamma\psi^{t+a}}. \quad (41)$$

Therefore, every $|e_i(t)|$ has an upper bound and will never exceed it. \square

4. Simulations, Comparisons, and Tests

In this section, for testing the reliability and accuracy of two models (23) and (33), we apply them to the PA10 mobile manipulator, respectively, with the task of running star-shaped as well as cardioid tracking paths when we take joint drifting phenomenon into consideration initially. Moreover, for the purpose of highlighting the superiority of the proposed model, the analysis compared with the ZNN model is also added. The ZNN model is described as follows:

$$\begin{aligned} \dot{Y}(t) = & -\dot{H}(t)Y(t) + (I - H(t))\dot{Y}(t) - \gamma\Phi(H(t)Y(t) \\ & - G(t)) + \dot{G}(t). \end{aligned} \quad (42)$$

In addition, considering the existence of external interference $\zeta(t)$, we have the following disturbed ZNN model:

$$\begin{aligned} \dot{Y}(t) = & -\dot{H}(t)Y(t) + (I - H(t))\dot{Y}(t) - \gamma\Phi(H(t)Y(t) \\ & - G(t)) + \dot{G}(t) + \zeta(t). \end{aligned} \quad (43)$$

In these simulations, we set $\eta_1 = \eta_2 = \eta_3 = k = 10$ in (13) uniformly. The radius of all three wheels is 10 cm, and point A on the mobile platform is 30 cm away from the center of the wheel. The initial state of the mobile base is set as $\alpha(0) = 0$ rad and $\rho(0) = [0, 0, 0]^T$. As for manipulator PA10, the desired initial joints are $\theta^*(0) = [0, -\pi/4, 0, \pi/2, 0, -\pi/4, 0]^T$, then the actual initial joints are $\theta(0) = [0, -\pi/4, 0, \pi/2, 0, 2-\pi/4, 0]^T$, and the sixth joint has been deviated 2 rad.

4.1. Star-Shaped Path Tracking Control. The end effector is expected to track a star-shaped path firstly. The relevant parameters of the EVPNN are $\gamma = 10$, $\psi = 2$, and $a = 1$. For a fair comparison, the related parameter γ is also set to 10 in (42) and (43). Then, we select a general linear function as the activation function, that is, $\Phi(E(t)) = E(t)$. The expression of the desired trajectory is shown as follows:

$$\begin{cases} r_x^*(t) = \cos^3\left(2\pi \cdot \sin\left(\frac{\pi t}{2T}\right)\right) + 0.0354, \\ r_y^*(t) = \sin^3\left(2\pi \cdot \sin\left(\frac{\pi t}{2T}\right)\right), \\ r_z^*(t) = 0.7518, \end{cases} \quad (44)$$

where T represents the task execution time, and $T = 10$ s in this simulation.

The corresponding simulation results of the EVPNN without noise are shown in Figures 3 and 4(a). Specifically, Figures 3(a) and 3(b) provide a vertical view and a horizontal view for the entire mobile manipulator, respectively. The desired trajectory and actual path of the end effector are shown in Figure 3(c) together. Figure 3(d) shows each joint angle profile, and it is clearly seen that proposed model (23) can make joints turn back to the desired initial position during the tracking task. As can be seen in Figure 4, the EVPNN model makes the end effector of PA10 accomplish star-shaped tracking path tasks excellently, and the final position error of the end effector in three dimensions is smaller than 2×10^{-5} m. Besides, the position error using ZNN model (42) is shown in Figure 4(b), and the final position error is only smaller than 2×10^{-3} m. Comparing the EVPNN model and ZNN model, the former is much better than the latter for mobile manipulator tracking control.

To demonstrate the robustness of model (33), Figure 5 shows the corresponding simulation results of disturbed ZNN (43) and EVPNN model (33) under the external noise $\zeta(t) = 0.1 \times [\sin(4t), \cos(4t), \dots, \cos(4t)]^T$. Figure 5(a) gives the desired trajectory and actual path of the end effector when using the EVPNN, and Figure 5(b) shows the desired trajectory and actual path of the end effector

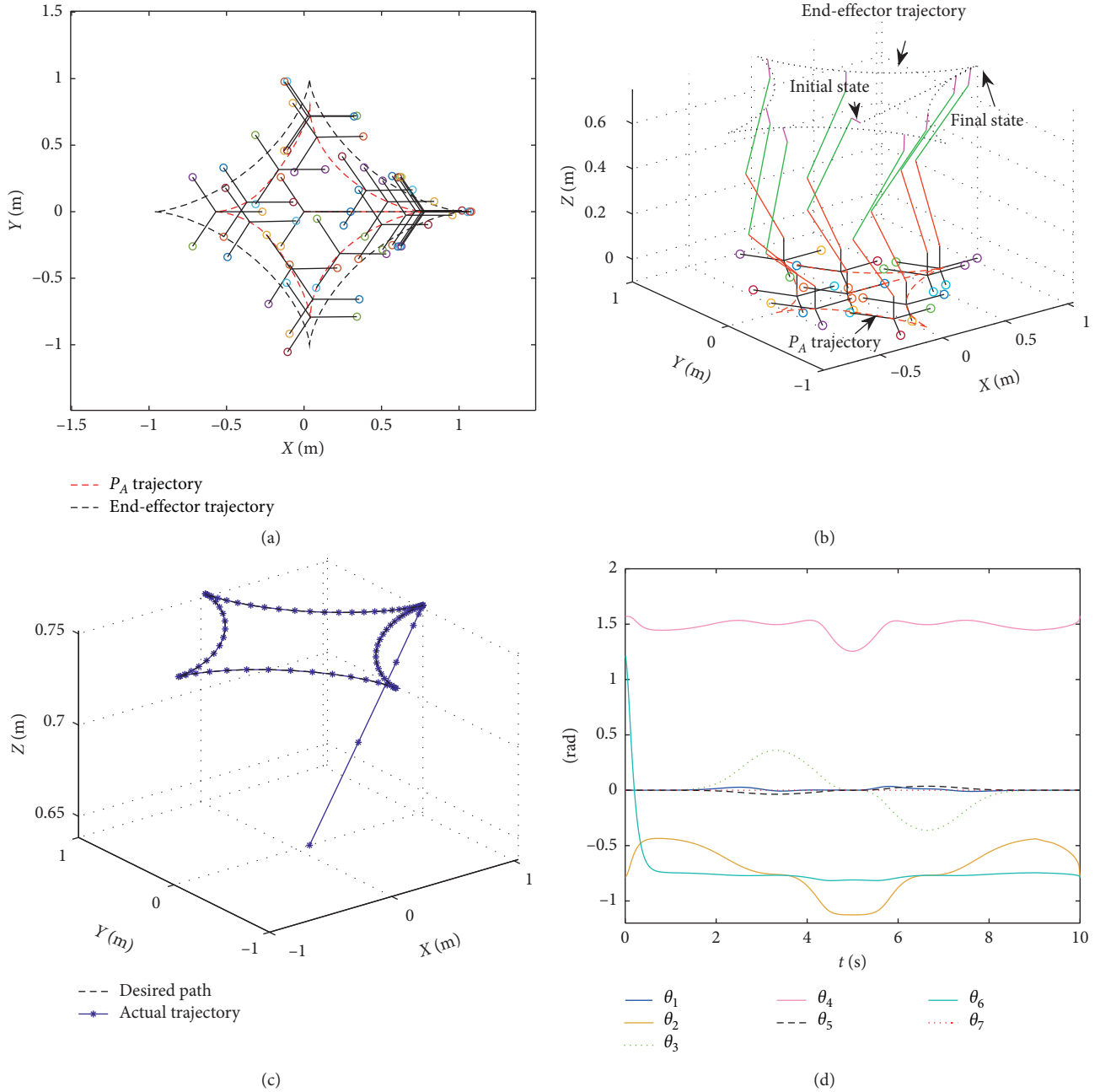


FIGURE 3: Simulation results of EVPNN model (23) without noise when the end effector of the PA10 mobile robot tracks the star-shaped path. (a) Top view of trajectories of the end effector and platform with three wheels. (b) Horizontal view for the entire mobile manipulator. (c) Desired path and actual trajectory. (d) Profiles of joint angles $\theta_1, \theta_2, \dots, \theta_7$.

when using the ZNN. It is obvious to see that the actual path of the EVPNN is very close to the desired trajectory, and the actual path of the ZNN cannot reach the desired trajectory on the contrary. Thus, EVPNN has much better robustness.

4.2. Cardioid Path Tracking Control. For further validating the model, this section is designed to track a cardioid path by the PA10 manipulator. The desired trajectory is

functioned from the x -axis, y -axis, and z -axis, which is listed as follows:

$$r_x^* = 3.2 \cos\left(2\pi \cdot \sin\left(\frac{\pi t}{2T}\right)\right) - 1.6 \cos\left(4\pi \cdot \sin\left(\frac{\pi t}{2T}\right)\right) + 0.0354,$$

$$r_y^* = 1.6 \sin\left(2\pi \cdot \sin\left(\frac{\pi t}{2T}\right)\right) - 0.8 \sin\left(2\pi \cdot \sin\left(\frac{\pi t}{2T}\right)\right),$$

$$r_z^* = 0.7518,$$

(45)

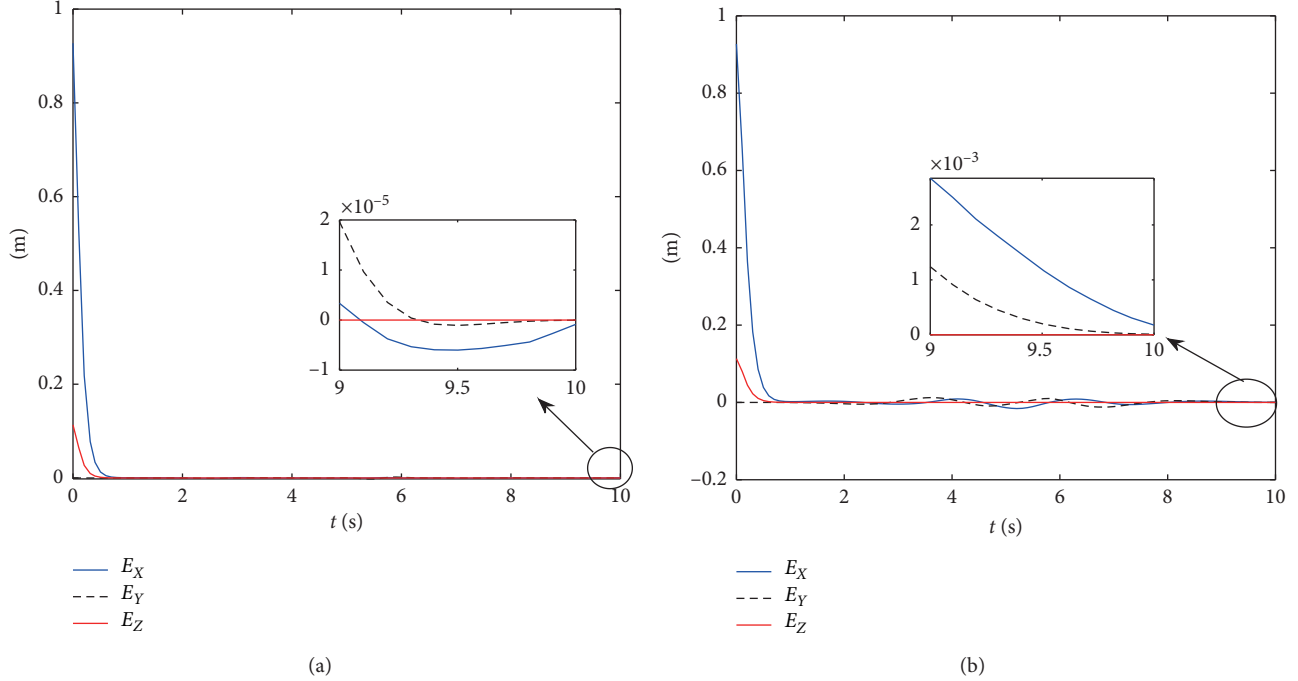


FIGURE 4: Synthesized positioning errors of the end effector by the EVPNN model and ZNN model when completing the task of the star-shaped path. (a) EVPNN model. (b) ZNN model.

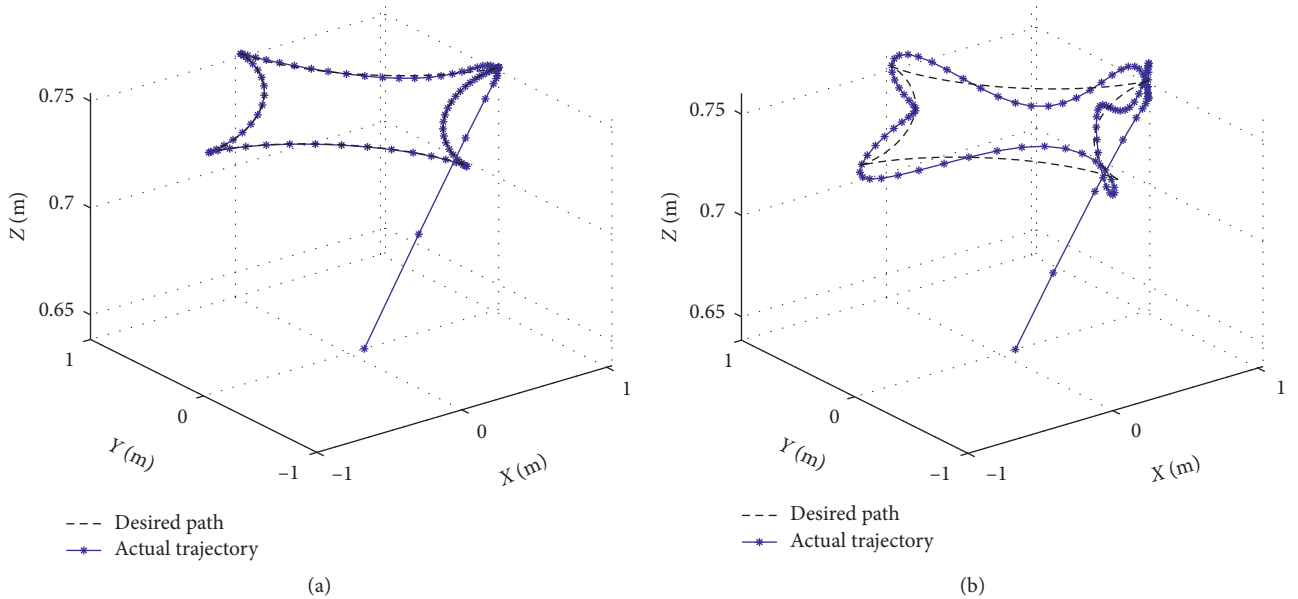


FIGURE 5: Desired path and actual trajectory synthesized by two models in the presence of vector-form noise. (a) Disturbed EVPNN model (33). (b) Disturbed ZNN model (43).

where T denotes the execution time, which is set to 10 s by default.

In this task, we choose the bipolar sigmoid function as the nonlinear activated function with parameter $\varepsilon = 3$. Furthermore, $\gamma = 10$, $\psi = 2$, and $a = 1$ are set the same as before. Consequently, the moving trails of the mobile base as well as the end effector from the top view angle and side-

looking angle are observed in Figures 6(a) and 6(b), respectively. Especially in Figure 6(b), the final completed trajectory is closed, even though the initial position is not on the predetermined one, namely, each joint angle will eventually approach to the initial wanted angle, thus completing the complex repetitive task. The movement changes of each joint angle in detail are depicted in Figure 6(d). From

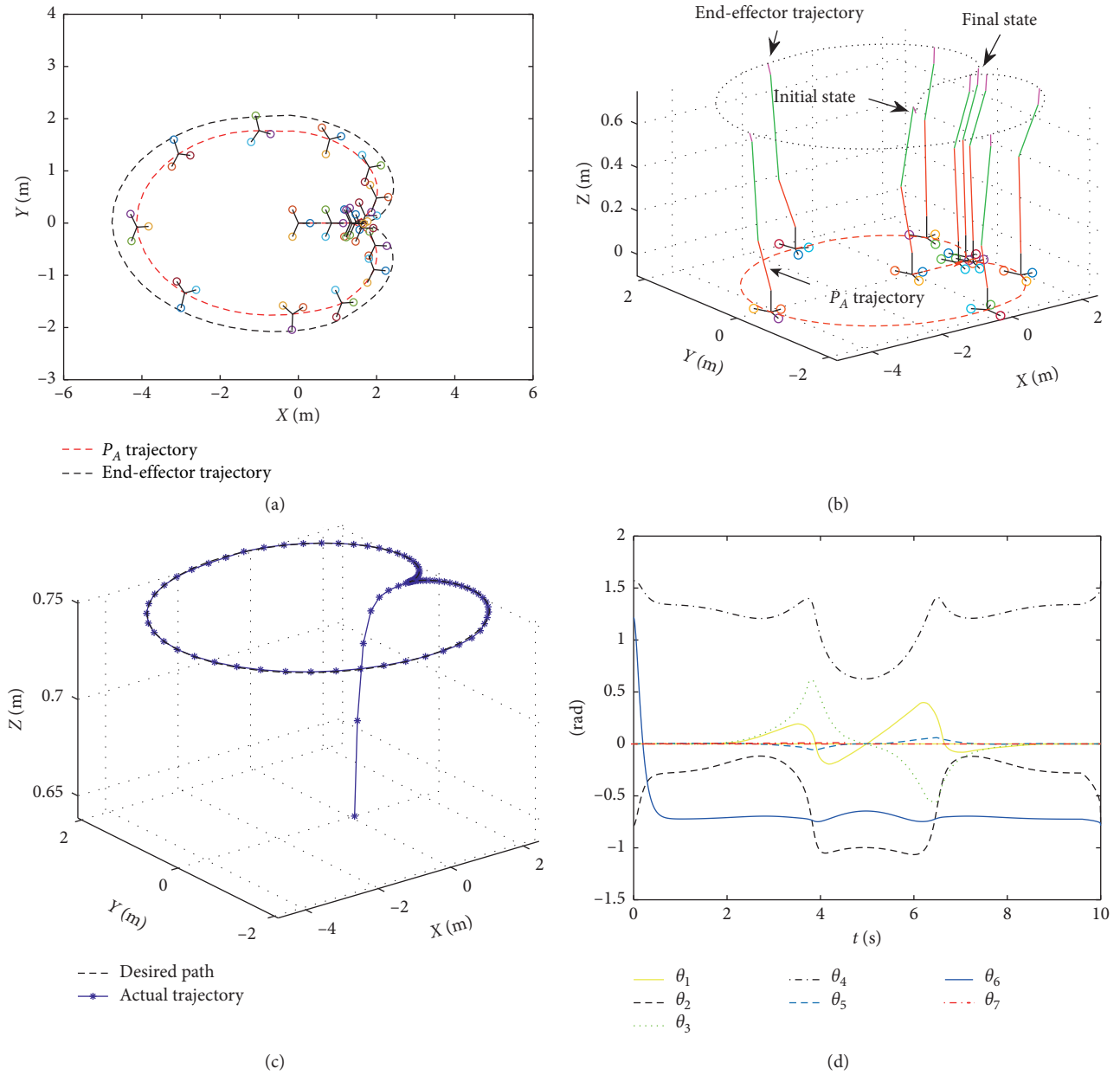


FIGURE 6: Simulation results of EVPNN model (23) without noise when the end effector of the PA10 mobile robot tracks the cardioid path. (a) Top view of trajectories of the end effector and platform with three wheels. (b) Horizontal view for the entire mobile manipulator. (c) Desired path and actual trajectory. (d) Profiles of joint angles $\theta_1, \theta_2, \dots, \theta_7$.

Figure 6(c), the dotted line representing the ideal path is completely coincident with the asterisk line representing the actual running one, regardless of the intentional deviation θ_6 at the beginning.

Comparing Figures 7(a) and 7(b), position errors composed by E_X, E_Y , and E_Z are all rapidly decreased to zero in 2 s. However, in ultimate 10 s, the error precision of the

ZNN model is less than 2×10^{-3} m, while that of Figure 7(a) is merely 10^{-5} m.

All of the above are simulated in an undisturbed environment. However, external interference is added in the following experiments. As seen from Figure 8(b), when the noise is considered, the ZNN model oscillates more obviously. That is to say, there is a large error between the desired

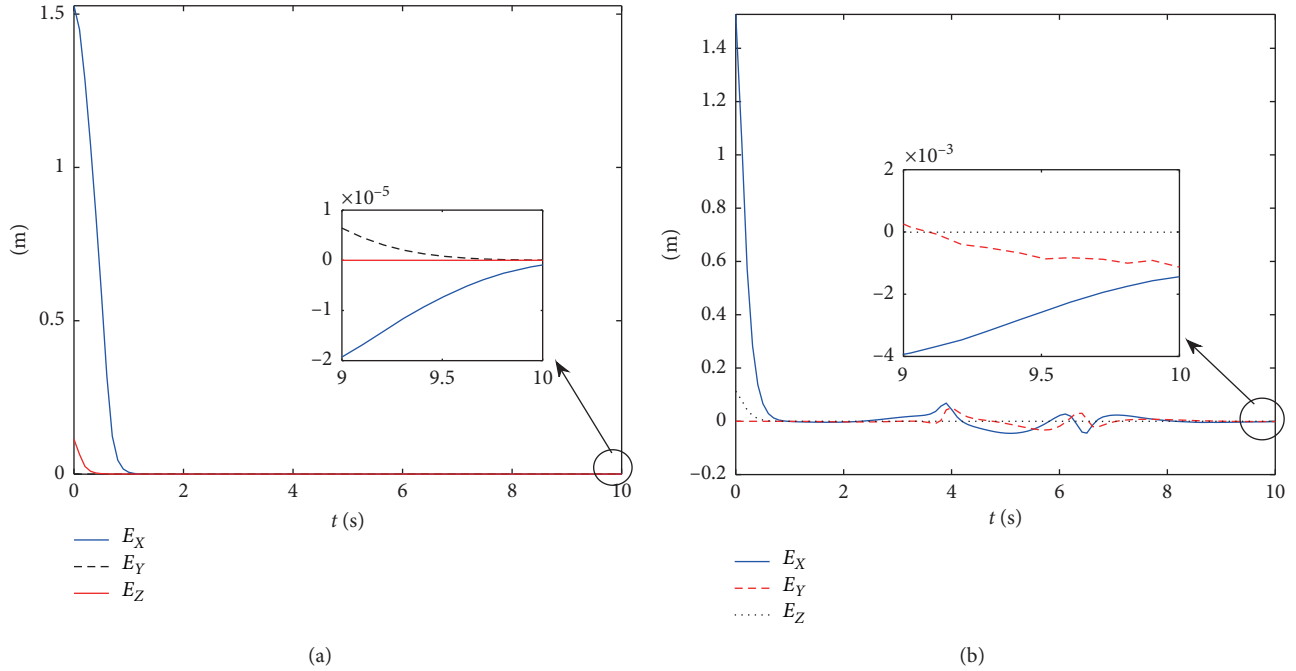


FIGURE 7: Synthesized positioning errors of the end effector by the EVPNN model and ZNN model when completing the task of the cardioid path. (a) EVPNN model. (b) ZNN model.

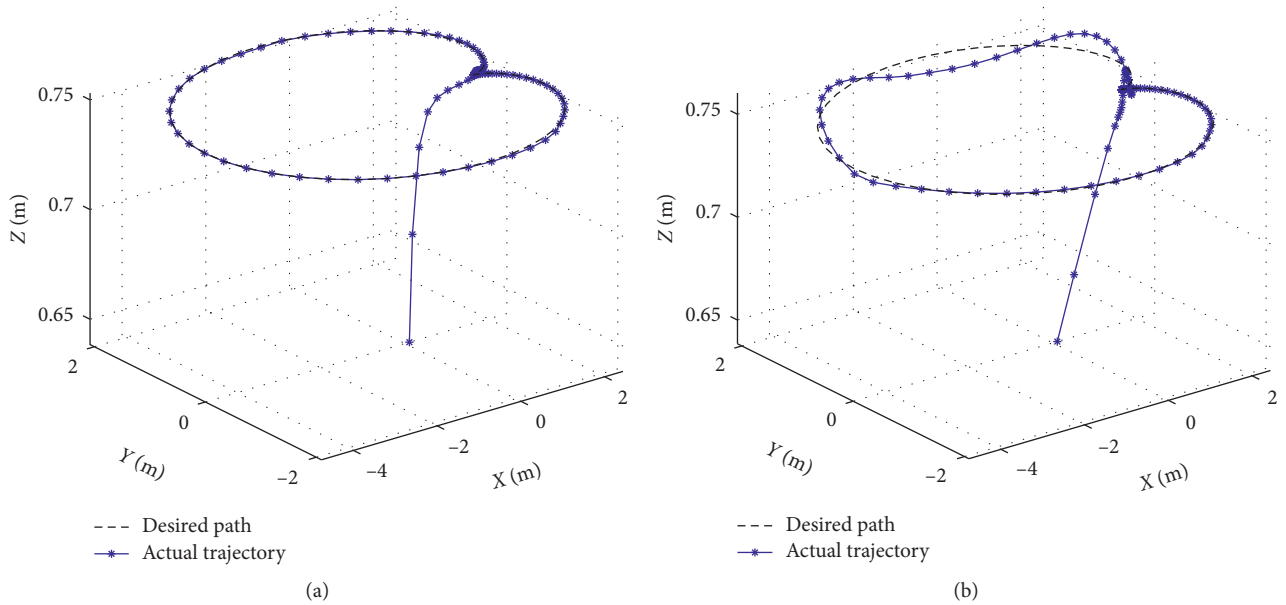


FIGURE 8: Desired path and actual trajectory synthesized by two models in the presence of vector-form noise. (a) Disturbed EVPNN model (33). (b) Disturbed ZNN model (43).

path and the actual trajectory. On the contrary, the disturbed EVPNN model shows a better robustness performance when tracking a closed cardioid path in Figure 8(a).

5. Conclusion

This paper is aimed at solving the problem of repetitive motion of the PA10 manipulator with a mobile base. After

analysis, it can be transformed into a quadratic programming problem mathematically. Then, the key point of this paper is to propose an improved QP solver that is EVPNN model (23). Next, we prove that the EVPNN model is stable globally and robust by theories. At last, two specific simulation examples have been practiced and thus verified that the proposed model can solve the motion planning problem of redundant mobile manipulator. Furthermore, we also

discuss the movement of the end effector with and without external interference and make some comparisons with existing ZNN model (42) as well as (43). The final experimental results show the superiority of the proposed model, that is to say, the EVPNN model possesses higher convergence accuracy and stronger anti-interference performance. However, most research works mainly focus on the continuous dynamic system. For the realization of potential hardware implementation, discrete-time algorithms may be investigated. It is worth mentioning that the EVPNN model can be applied to mathematical calculations, control problems, and electronic circuits.

Data Availability

The source code and source data can be provided by contacting with the corresponding author.

Conflicts of Interest

The authors declare that there are no conflicts of interest regarding the publication of this paper.

Acknowledgments

This study was partly supported by the National Natural Science Foundation of China (Grant nos. 61803338, 61972357, and 61672337), the Zhejiang Provincial Natural Science Foundation of China (Grant no. LGG18F020011), and Zhejiang Key R&D Program (Grant no. 2019C03135).

References

- [1] W. Ye, Z. Li, C. Yang, J. Sun, C.-Y. Su, and R. Lu, "Vision-based human tracking control of a wheeled inverted pendulum robot," *IEEE Trans Cybern*, vol. 46, no. 11, p. 24232434, 2016.
- [2] Q. Chen, H. Shi, and M. Sun, "Echo state network based backstepping adaptive iterative learning control for strict-feedback systems: an error-tracking approach," *IEEE Trans Cybern*, vol. 2, no. 93, p. 114, 2019.
- [3] C. Wei, M. Benosman, and T. Kim, "Online parameter identification for state of power prediction of lithium-ion batteries in electric vehicles using extremum seeking," *International Journal of Control, Automation and Systems*, vol. 17, no. 11, pp. 2906–2916, 2019.
- [4] G. Hu, N. Gans, N. Fitz-Coy, and W. Dixon, "Adaptive homography based visual servo tracking control via a quaternion formulation," *IEEE Transactions on Control Systems Technology*, vol. 18, no. 1, p. 128135, 2010.
- [5] L. Li, S. Yan, X. Yu, Y. K. Tan, and H. Li, "Robust multiperson detection and tracking for mobile service and social robots," *IEEE Transactions on Systems, Man, and Cybernetics*, vol. 42, no. 5, p. 13981412, 2012.
- [6] S. Li, Z. Wang, and Y. Li, "Using laplacian eigenmap as heuristic information to solve nonlinear constraints defined on a graph and its application in distributed range-free localization of wireless sensor networks," *Neural Processing Letters*, vol. 34, no. 6, pp. 411–424, 2013.
- [7] C. Yang, Y. Jiang, Z. Li, and W. He, "Neural control of bimanual robots with guaranteed global stability and motion precision," *IEEE Transactions on Industrial Informatics*, vol. 28, no. 2, pp. 415–428, 2017.
- [8] D. Chen, S. Li, W. Li, and Q. Wu, "A multi-Level simultaneous minimization scheme applied to jerk-bounded redundant robot manipulators," *IEEE Transactions on Automation Science and Engineering*, vol. 17, no. 1, pp. 463–474, 2020.
- [9] O. Linda and M. Manic, "Self-organizing fuzzy haptic teleoperation of mobile robot using sparse sonar data," *IEEE Transactions on Industrial Electronics*, vol. 58, no. 8, p. 31873195, 2011.
- [10] Q. Chen, S. Xie, M. Sun, and X. He, "Adaptive nonsingular fixed-time attitude stabilization of uncertain spacecraft," *IEEE Transactions on Aerospace and Electronic Systems*, vol. 54, no. 6, pp. 2937–2950, 2018.
- [11] K. Tchon, "Repeatability of inverse kinematics algorithms for mobile manipulators," *IEEE Transactions on Automation Science and Engineering*, vol. 47, no. 8, p. 13761380, 2002.
- [12] K. Tchon and J. Jakubiak, "Endogenous configuration space approach to mobile manipulators: a derivation and performance assessment of Jacobian inverse kinematics algorithms," *International Journal of Control, Automation and Systems*, vol. 76, no. 14, p. 13871419, 2003.
- [13] K. Tchon and J. Jakubiak, "A repeatable inverse kinematics algorithm with linear invariant subspaces for mobile manipulators," *IEEE Transactions on Systems, Man, and Cybernetics*, vol. 35, no. 5, p. 10511057, 2005.
- [14] K. Tchon, "Repeatable, extended Jacobian inverse kinematics algorithm for mobile manipulators," *Systems & Control Letters*, vol. 55, no. 2, p. 8793, 2006.
- [15] W. He, S. S. Ge, Y. Li, E. Chew, and Y. S. Ng, "Neural network control of a rehabilitation robot by state and output feedback," *Journal of Intelligent and Robotic Systems*, vol. 80, no. 1, p. 1531, 2015.
- [16] J. Na, B. Wang, G. Li, S. Zhan, and W. He, "Nonlinear constrained optimal control of wave energy converters with adaptive dynamic programming," *IEEE Transactions on Industrial Electronics*, vol. 66, no. 10, pp. 7904–7915, 2019.
- [17] J. Na, Y. Huang, X. Wu, S. Su, and G. Li, "Adaptive finite-time fuzzy control of nonlinear active suspension systems with input delay," *IEEE Trans Cybern*, vol. 50, no. 6, pp. 2639–2650, 2019.
- [18] J. Na, A. Chen, and Y. Huang, "Air-fuel ratio control of internal combustion engines with unknown dynamics estimator: theory and experiments," *IEEE Transactions on Control Systems Technology*, 2019.
- [19] S. Wang, L. Tao, Q. Chen, J. Na, and X. Ren, "USDE-based sliding mode control for servo mechanisms with unknown system dynamics," *IEEE/ASME Transactions on Mechatronics*, vol. 25, no. 2, pp. 1056–1066, 2020.
- [20] W. He, Y. Ouyang, and J. Hong, "Vibration control of a flexible robotic manipulator in the presence of input dead-zone," *IEEE Transactions on Industrial Informatics*, vol. 13, no. 1, p. 4859, 2017.
- [21] Y. Zhang, C. Yi, D. Guo, and J. Zheng, "Comparison on Zhang neural dynamics and gradient-based neural dynamics for online solution of nonlinear time-varying equation," *Neural Computing and Applications*, vol. 20, no. 1, pp. 1–7, 2011.
- [22] Y. Zhang and S. Ge, "Design and analysis of a general recurrent neural network model for time-varying matrix inversion," *IEEE Transactions on Neural Networks and Learning Systems*, vol. 16, no. 6, pp. 1447–1462, 2005.
- [23] Y. Zhang, X. Yan, D. Chen, and D. Guo, "QP-based refined manipulability-maximizing scheme for coordinated motion planning and control of physically constrained wheeled

- mobile redundant manipulators,” *Nonlinear Dynamics*, vol. 85, no. 5, pp. 245–261, 2016.
- [24] Y. Shen, P. Miao, Y. Huang, and Y. Shen, “Finite-time stability and its application for solving time-varying Sylvester equation by recurrent neural network,” *Neural Processing Letters*, vol. 42, no. 10, pp. 763–784, 2015.
- [25] P. Miao, Y. Shen, and X. Xia, “Finite time dual neural networks with a tunable activation function for solving quadratic programming problems and its application,” *Neurocomputing*, vol. 143, no. 16, pp. 80–89, 2014.
- [26] L. Xiao, B. Liao, S. Li, and K. Chen, “Nonlinear recurrent neural networks for finite-time solution of general time-varying linear matrix equations,” *Neural Networks*, vol. 98, pp. 102–113, 2018.
- [27] S. Li, S. Chen, and B. Liu, “Accelerating a recurrent neural network to finite-time convergence for solving time-varying Sylvester equation by using a sign-Bi-power activation function,” *Neural Processing Letters*, vol. 37, no. 2, pp. 189–205, 2013.
- [28] L. Xiao, “A finite-time recurrent neural network for solving online time-varying Sylvester matrix equation based on a new evolution formula,” *Nonlinear Dynamics*, vol. 90, no. 3, pp. 1581–1591, 2017.
- [29] D. Chen and Y. Zhang, “Robust zeroing neural-dynamics and its time-varying disturbances suppression model applied to mobile robot manipulators,” *IEEE Transactions on Neural Networks and Learning Systems*, vol. 29, no. 9, pp. 4385–4397, 2018.
- [30] Z. Zhang, L. Zheng, J. Yu, Y. Li, and Z. Yu, “Three recurrent neural networks and three numerical methods for solving repetitive motion planning scheme of redundant robot manipulators,” *IEEE/ASME Transactions on Mechatronics*, vol. 22, no. 3, p. 14231434, 2017.
- [31] L. Jin and Y. Zhang, “G2-type SRMPC scheme for synchronous manipulation of two redundant robot arms,” *IEEE Trans Cybern*, vol. 45, no. 2, p. 153164, 2015.
- [32] S. Li, S. Chen, B. Liu, Y. Li, and Y. Liang, “Decentralized kinematic control of a class of collaborative redundant manipulators via recurrent neural networks,” *Neurocomputing*, vol. 91, no. 23, pp. 1–10, 2012.
- [33] S. Li, J. He, Y. Li, and M. U. Rafique, “Distributed recurrent neural networks for cooperative control of manipulators: a game-theoretic perspective,” *IEEE Transactions on Neural Networks and Learning Systems*, vol. 28, no. 2, pp. 415–426, 2017.
- [34] Y. Zhang, H. Wu, D. Guo, L. Xiao, and H. Zhu, “The link and comparison between velocity-level and acceleration-level repetitive motion planning schemes verified via PA10 robot arm,” *Mechanism and Machine Theory*, vol. 69, pp. 245–262, 2013.
- [35] Y. Zhang, W. Li, and B. Liao, “Analysis and verification of repetitive motion planning and feedback control for omnidirectional mobile manipulator robotic systems,” *International Journal of Advanced Robotic Systems*, vol. 75, no. 3-4, pp. 393–411, 2014.